A Theoretical Study of the S + C_2H Reaction: Potential Energy Surfaces and Dynamics

J. R. Flores,* C. M. Estévez, L. Carballeira, and I. Pérez Juste

Departamento de Química Física, Facultad de Ciencias, Campus de Vigo, Universidad de Vigo, 36200-Vigo, Spain

Received: November 10, 2000; In Final Form: January 22, 2001

A theoretical study of the reaction of S with C_2H has been carried out. This reaction is a possible step in the generation of sulfur-containing cumulenes in interstellar clouds and circumstellar envelopes. The potential energy surfaces were computed by means of the G2, G2(QCI), and CBS-Q methods in the case of local minima and saddle points. The energy profiles for the interaction of S and C_2H in all states associated with the lowest energy electron configurations have received special attention. The MR-AQCC/aug-cc-pVTZ method was used as the basic level of computation; spin−orbit interactions and basis set superposition corrections were also taken into account. We found only two neatly attractive potential energy surfaces, corresponding to the $^2\Pi_{3/2}$ and $^2\Pi_{1/2}$ electronic states. We employed an approximate classical trajectory method to compute the capture rate. According to our computations the reaction is relatively fast, its rate for $T = 300$ K being not too far from the typical values for ion−molecule reactions. The main product should be $SC_2(^3\Sigma^-)+H(^2S)$. However, we have encountered a slight decrease in the rate coefficient with decreasing temperature.

I. Introduction

A number of carbon chain molecules have been detected in interstellar space: linear unsaturated hydrocarbons C_nH_2 ($n = 2-4$), C_nH ($n = 1-6$), cyanopolyyines HC_nN ($n = 1-11$), C_n ($n = 2-5$), carboxylpolyyines C_nO ($n = 1-5$), and the analogous sulfur-containing counterparts C_nS($n = 1-3$).[1,2] The sulfur-containing molecules have been identified in dark clouds like TMC-1[3,4,5] and in the IRC+10216[6] circumstellar envelope; there is also a tentative detection of C_5S in IRC+10216.[7]

Some sulfur-containing carbon chains (C_nS and SC_nS, $n = 1-5$) have been produced by Vala and co-workers[8] by pulsed laser ablation of a carbon/sulfur mixture deposited in an Ar matrix and studied through Fourier transform infrared absorption spectroscopy. Maier and co-workers generated also some of these compounds by flash photolysis and flash pyrolysis of cyclic sulfur-containing compounds in Ar matrices, and detected them by infrared absorption spectroscopy.[9] The groups of Lovas,[10] Oshima,[11] Hirahara,[12] and Kasai[13] have generated C_2S and C_3S by high voltage discharge of gaseous mixtures in a Fabry−Perot cavity and recorded microwave spectra. There are several studies of the tioketyl radical, SCCH, the optical spectrum,[14,15] laser-induced fluorescence,[16] and rotational spectrum[17] have been recorded. Among the recent theoretical studies on SC_2 we will cite the work of Lee,[18] who used a BLYP method, the work of Vala and co-workers,[8] who employed both B3LYP and MP2 approaches, and the older but high-quality CI computations of Schaefer and Xie.[19] There are also some recent theoretical studies on the lowest-lying states of SC_2H in its linear conformation.[20,21,22]

The reaction mechanisms proposed for the generation of sulfur-containing chains in dense interstellar clouds involve bimolecular gas-phase reactions of S^+ with hydrocarbons followed by dissociative recombination steps,[1,23] for instance:

$$S^+ + C_2H_2 \rightarrow SC_2H^+ + H$$

$$SC_2H^+ + e^- \rightarrow SC_2 + H$$

The main reason supporting this type of mechanism is that S^+ is unable to react with molecular hydrogen. However, C_2S and C_3S have also been detected in circumstellar envelopes and here neutral−neutral reactions must not be excluded.[24] It should also be noted that Vala and co-workers have concluded that some neutral−neutral reactions, rather than reactions involving S^+, were responsible for their formation.[8]

The aim of the present work is to study the simplest case of an interesting alternative,[25] namely, the reactions of sulfur with C_nH radicals; in other words we will study the following reaction:

$$S + C_2H \rightarrow C_2S + H$$

The objectives of this paper are an ab initio study of the lowest lying potential surfaces of the (SC_2H) system, as well as a preliminary study of the reaction dynamics, to establish whether it can be a fast process in the conditions prevailing in the dark interstellar clouds and circumstellar envelopes.

It must be noted that reactions of small hydrocarbons and hydrocarbon radicals have been the subject of some recent theoretical studies by Herbst and Woon, which also include the treatment of their dynamical behavior.[26,27]

II. Computational Details of the ab Initio Computations

All local minima and saddle points have been computed at the Gaussian-2 (G2)[28] and CBS-Q[29] levels. In addition, we used a Gaussian-style method closely related to the G2(QCI) method[30] in order to obtain more reliable energy differences between minima and saddle points of the same potential surface. It may be described as follows:

* To whom correspondence should be addressed. E-mail: flores@uvigo.es.

10.1021/jp004169a CCC: $20.00
Published on Web 04/24/2001

•Geometry optimizations were carried out at the QCISD/6-311++G** level without enforcing any symmetry unless we indicate the opposite.

•Vibrational frequencies were obtained at the MP2=full/6-31G* level

•Electronic energies were determined at the QCISD(T)/6-311+G(3df,2p) level using the QCISD/6-311++G** geometries.

•The so-called high-level correction was defined as in the G2(QCI) approach.

The uses of MP2=full/6-31G* frequencies (instead of scaled HF/6-31G* frequencies employed in the original G2(QCI) approach) and QCISD/6-311++G** optimized geometries (instead of MP2=full/6-31G* ones) are considered more adequate options in the case of saddle points (the superiority of the QCI method over the MP2 method for obtaining saddle point geometries has already been established[31]).

The reaction coordinate for the interaction of S with the C_2H radical has been determined by means of geometry optimizations for a series of fixed S−C distances, i.e., the distance between sulfur and the carbon atom not bonded to hydrogen. These optimizations were performed at the B3LYP/6-311++G** level within $C_{\infty v}$ symmetry. In the choice of this approach we valued the fact that B3LYP wavefuntions are almost spin-pure for geometries close to the minimum, and also that the computation is quite cheap in terms of computer time even if stringent accuracy requirements are employed. Using this set of geometries we performed averaged quadratic coupled-cluster (AQCC) computations. The AQCC method[32] can be considered a variant of the ACPF (averaged coupled-pair functional) method,[33] which can be viewed as a size consistent MRCI method. The AQCC wave functions included all single and double spin−orbital substitutions in the reference wave function, leaving aside core orbitals. The reference wave function was a MCSCF wave function including the following configurations:

$$^2\Pi:\ [..3\pi^3\ 9\sigma^2],\ [..3\pi^3\ 10\sigma^2],\ [..3\pi^3\ 9\sigma^1\ 10\sigma^1]\ (C_{\infty v})$$

$$^2B_1:\ [..3b_1{}^1 9a_1{}^2],\ [..3b_1{}^1 10a_1{}^2],\ [..3b_1{}^1 9a_1{}^1 10a_1{}^1]\ (C_{2v})$$

Both the AQCC and MCSCF computations were carried out enforcing only C_{2v} symmetry. The correlation consistent aug-cc-pVTZ basis set was used.[34]

The MCSCF and MRCI-type computations have been made with the COLUMBUS program system[35] and, in most cases, with the MOLPRO program package;[36] the rest of the ab initio computations have been carried out with the GAUSSIAN 94[37] and GAUSSIAN 98 program packages.[38]

We studied the electronic structure of the reaction intermediates by means of the natural bond orbital (NBO) analysis, which describes the formation of new bonds in terms of natural hybrids of the interacting atoms. To keep consistency with the geometrical results, the NBO method was applied on the QCISD/6-311+G**//QCISD/6-311++G** wave functions. The analysis of the HF/6-31G*//QCISD/6-311++G** wave functions was also performed in order to estimate the impact of the stabilization due to the interactions between orbitals (it must be recalled here that the NBO energetic analysis can be only applied on Hartree−Fock type wave functions).[39]

III. The PES of the (SC_2H) System

We found four stable species, namely, in increasing energy order: SCCH($^2\Pi$), $SC_2H(^2A'')$, HSCC($^2A''$), and SCHC($^2A'$). The QCISD/6-311++G(d,p) optimized geometries are shown in Figure 1. The relative energies are given in Table 1. Schemes 1 and 2 are diagrams where reactants, products, local minima, and saddle points are placed according to their energy and connected with lines that represent processes. It is readily seen that SCCH($^2\Pi$) is the ground state and a relatively deep minimum. This state correlates with the ground-state reactants $S(^3P)+C_2H(^2\Sigma^+)$. It has already been pointed out that this state must experience the Renner-Teller effect;[20,21] it leads to the $^2A'$ and $^2A''$ electronic states if the linear conformation is distorted into planar geometries. The geometrical data indicate that the triple C−C bond is only slightly weakened when the S−C bond is formed, as reflected in the small increase of the bond length (1.234 Å vs 1.217 Å in $C_2H(^2\Sigma^+)$). According to the NBO analysis, the unpaired electron is mainly associated with sulfur and the structure is clearly stabilized by donation of electron density of the sulfur lone pairs into the π_{C-C} system (i.e., the NBO energetic analysis gives a stabilization energy of 42.4 kcal/mol for the $Lp(S)-\pi^*_{C-C}$ orbital interactions). SCCH($^2\Pi$) may rearrange into $SC_2H(^2A'')$ through the transition structure TS12($^2A''$). According to the normal mode of the imaginary vibrational frequency, this rearrangement involves the migration of both sulfur and hydrogen, which ends up bonded to the other carbon atom. SCCH($^2\Pi$) may also isomerize into SCHC($^2A'$) through TS14($^2A'$).

$SC_2H(^2A'')$ is a cyclic species, which lies about 27 kcal/mol above the ground state. It is interesting to note that the cyclic conformation is a result of the inclusion of electron correlation; with the UHF method one obtains an open structure, the $<SC_HC$ angle is 107.8° at the UHF/6-31G(d) level (C_H being the carbon atom holding hydrogen). Geometrical data and NBO results suggest that the electron density is more delocalized along the $S-C_H$-C frame in $SC_2H(^2A'')$ than in TS12($^2A''$), which results in a more stable structure. For $SC_2H(^2A'')$ the NBO method detects a σ_{S-C} bond, as well as $S-C_H$ and $C-C_H$ bonds with partial double bond character; the populations are 0.9216, 2.5966 and 2.9188, respectively. In contrast, only a single $S-C_H$ bond and a double C−C bond with populations 1.9402 and 3.7526, respectively, are found in TS12($^2A''$). The fact that the C−C bond length is slightly longer in $SC_2H(^2A'')$ (1.341 Å) than in TS12($^2A''$) (1.325 Å) agrees with the corresponding bond populations.

The lowest lying $^2A'$ state has a noncyclic conformation, which is peculiar in the fact that the <HCC angle is relatively small and the C−H bond is relatively long. It is worth noting that the $^2A''$ state lies below the $^2A'$ state at this geometry. The $^2A'$ minimum was reached through partial optimizations within planar geometries. The assumption that SCHC($^2A'$) is indeed a minimum has been confirmed by means of a series of MCSCF/6-311++G** computations for slightly nonplanar geometries in which the second root (i.e., the first excited state) was obtained. The NBO analysis shows the same description in terms of natural bond orbitals for SCHC($^2A'$) and TS12($^2A''$) (i.e., a single $S-C_H$ bond, a double C_H-C bond and a single C_H-H bond, with the unpaired electron mainly localized on sulfur). TS12($^2A''$) has a smaller C−H bond population (1.8377 vs 1.8797 in SCHC($^2A'$)) and a larger S−C bond population (1.9402 vs 1.9325 in SCHC($^2A'$)). The geometries are consistent with these electronic structure features: the C−H bond is larger in TS12($^2A''$) than that in SCHC($^2A'$) (1.124 and 1.102 Å, respectively), whereas the S−C bond is shorter (1.697 Å vs 1.744 Å in SCHC($^2A'$)). In addition, the NBO energetic analysis indicates that orbital interactions in TS12($^2A''$) are notably larger than in SCHC($^2A'$). For instance, in TS12($^2A''$), an energy of 41.3 kcal/mol is assigned to the interaction between the π_{C-C} orbital and

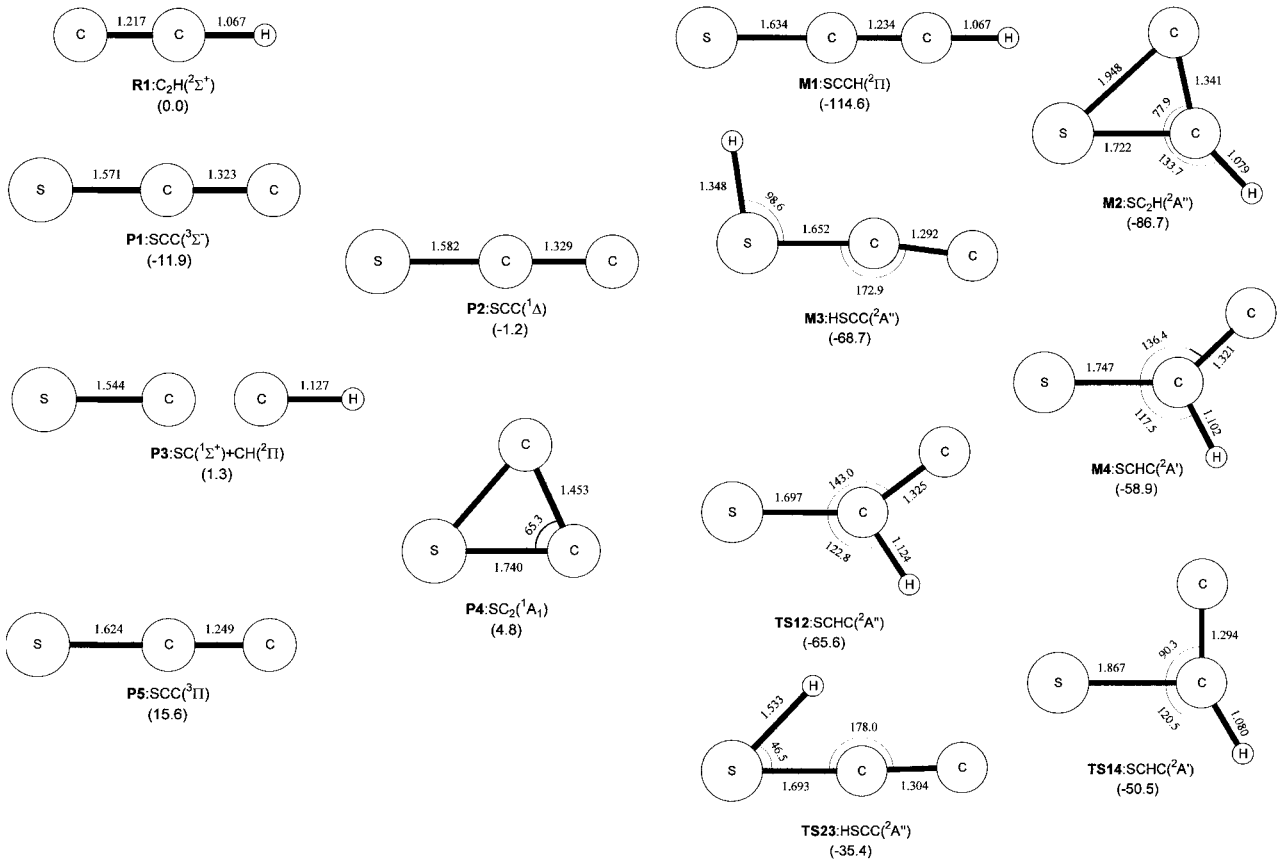

Figure 1. QCISD/6-311++G** optimized geometries for the local minima and saddle points of the lowest-lying electronic states of the SC_2H system. Bond distances are given in angstroms, and angles are given in degrees. G2(QCI) relative energies (kcal/mol, $T = 0$ K) are given in parentheses.

TABLE 1: Relative Energies in Kcal/Mol of Reactants, Products, Minima, and Saddle Points

species	G2 ΔU (0 K)	G2 ΔH (298 K)	CBS-Q ΔU (0 K)	CBS-Q ΔH(298 K)	G2(QCI) ΔU (0 K)
$S(^3P)+C_2H(^2\Sigma^+)$[a]	0.0	0.0	0.0	0.0	0.0
$SCC(^3\Sigma^-)+H(^2S)$	−10.1	−9.9	−12.8	−12.5	−11.9
$SCC(^1\Delta)+H(^2S)$	0.1	0.4	0.7	0.9	−1.2
$SC_2(^1A_1)+H(^2S)$	5.9	6.1	8.3	8.5	4.8
$SCC(^3\Pi)+H(^2S)$	16.8	17.1	13.4	13.7	15.6
$SC(^1\Sigma^+)+CH(^2\Pi)$	2.8	3.1	4.7	5.0	1.3
$HSCC(^2A'')$	−68.1	−68.8	−69.2	−69.9	−68.7
$SCHC(^2A')$	−54.1	−55.1	−55.4	−56.4	−58.9
$SC_2H(^2A'')$	−87.2	−88.1	−87.1	−88.0	−86.7
$SCCH(^2\Pi)$	−114.5	−115.4	−118.0	−119.0	−114.6
$TS12(^2A'')$	−65.2	−66.3	−66.2	−67.3	−65.6
$TS14(^2A')$	−55.1	−51.7	−53.5	−51.0	−50.5
$TS23(^2A")$	−36.4	−37.1	−37.9	−38.7	−35.4

[a] The absolute energies are −472.127976 (G2(0 K)), −474.133797 (CBS-Q(0 K)), −474,127464 (G2(QCI)).

the semi-occupied orbitals of sulfur; this kind of interaction is absent in $SCHC(^2A')$. According to the previous discussion, the higher degree of electron delocalization may explain why the $TS12(^2A'')$ lies below $SCHC(^2A')$.

$HSCC(^2A'')$ has an almost linear SCC group ($\angle SCC = 172.9°$). The existence of a strong C−C bond makes this state quite stable; in fact, it is about 14 kcal/mol lower in energy than $SCHC(^2A')$. The NBO analysis shows that the unpaired electron is mainly located at sulfur, just as in $SCCH(^2\Pi)$. However, there is a much higher degree of electron delocalization in $HSCC(^2A'')$; this causes the S−C bond to present partial double character (the population of the π_{S-C} orbital is 0.9322). As a consequence, the C−C bond is average between double and a triple, being longer (1.292 Å) than the C−C bonds in $C_2H(^2\Sigma^+)$ or $SCCH(^2\Pi)$.

$SC_2H(^2A'')$ may isomerize into $HSCC(^2A'')$ through $TS23(^2A'')$; this saddle point lies about 51 kcal/mol above the former species. $HSCC(^2A'')$ may undergo a S−H bond breaking process that would produce $SCC(^3\Sigma^-)+H(^2S)$; we could not find a neat saddle point for this process. We also tried to locate a saddle point that would connect directly $SC_2H(^2A'')$ with $SCC(^3\Sigma^-)+H(^2S)$, but all attempts led to $TS23(^2A'')$.

$SCHC(^2A')$ correlates with $SCC(^1\Delta)+H(^2S)$ for planar geometries. However, the interaction of the $^2A'$ and $^2A''$ states for nonplanar geometries in the vicinity of the $SCHC(^2A')$ minimum may make it possible for the latter species to lead to $SCC(^3\Sigma^-)+H(^2S)$ through a reaction coordinate of nonplanar geometries. This possibility is marked in Scheme 2 as a broken line.

Note that $SCCH(^2\Pi)$ correlates with $SCC(^3\Pi)$ for linear geometries, the latter species is about 27 kcal/mol higher than

SCHEME 1: Schematic Representation of the Lowest Lying $^2A-A''$ PES of the SC_2H System[a]

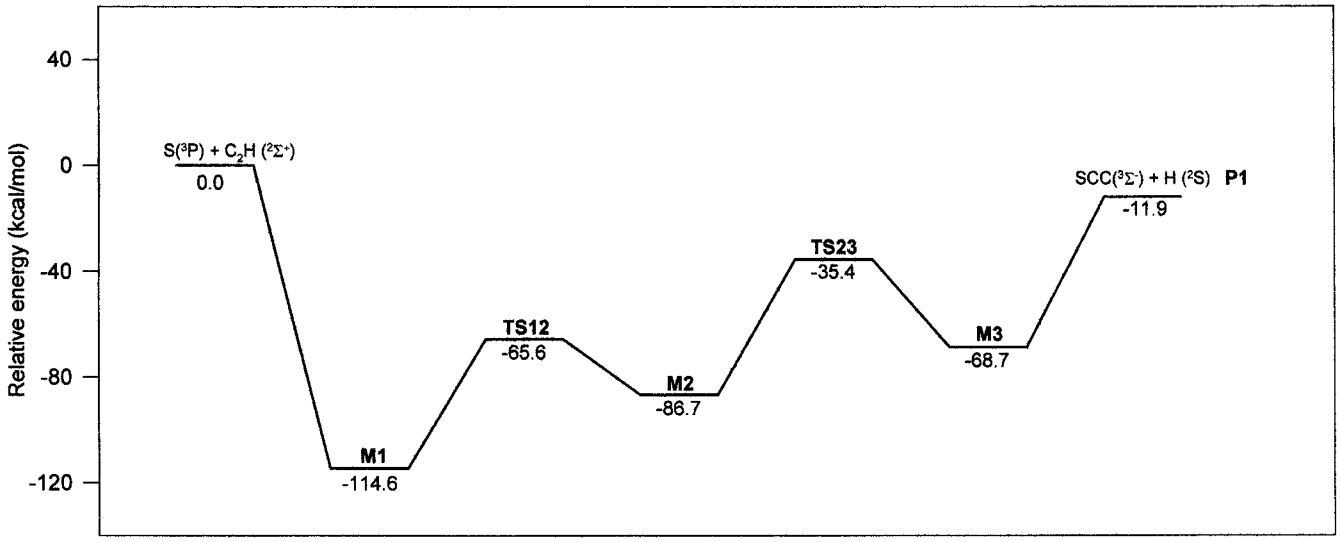

[a] The values indicate relative energies computed at the G2(QCI) level for $T = 0$ K given in kcal/mol.

SCHEME 2: Schematic Representation of the Lowest Lying $^2A-^2A'$ PES of the SC_2H System[a]

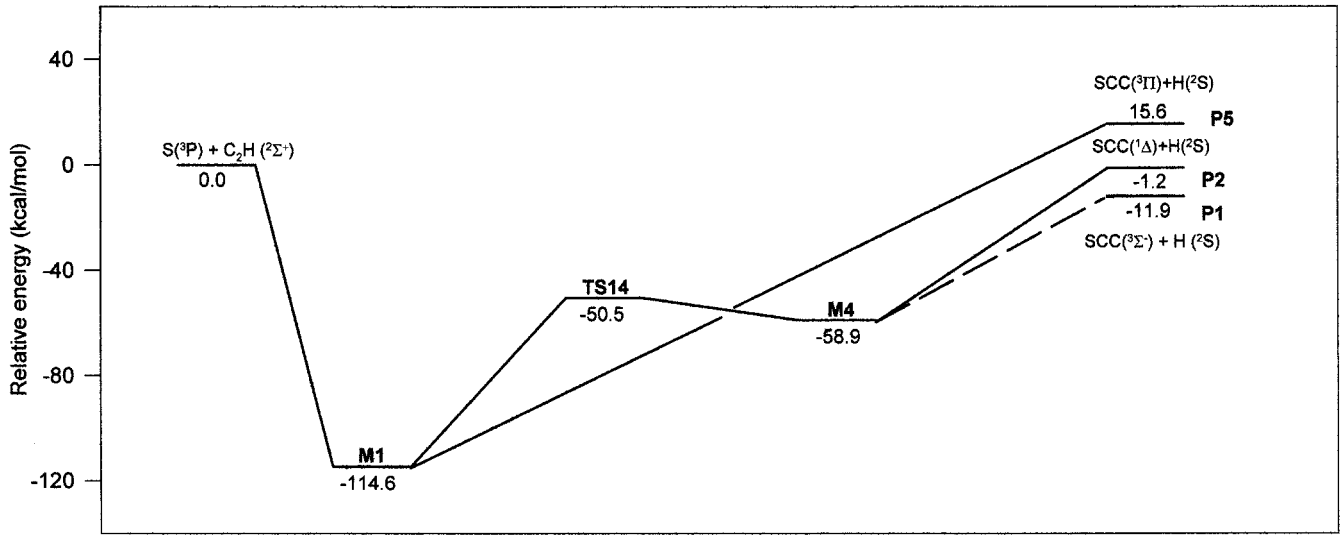

[a] The values indicate relative energies computed at the G2(QCI) level for $T = 0$ K given in kcal/mol.

$SCC(^3\Sigma^-)$ at the G2 level. However, the only obvious exothermic reaction channel is the one giving $SCC(^3\Sigma^-)+H(^2S)$.

Production of $SCC(^1\Delta)+H(^2S)$ appears to be exothermic only at the G2(QCI) level and by only −1.2 kcal/mol; this magnitude is close to the error expected for Guassian-type and CBS-type computations. It must be pointed out that the reference wave functions employed in the correlation computations made in the G2, G2(QCI) and CBS-Q calculations for $SCC(^1\Delta)$ represent a mixture of the $^1\Sigma^+$ and $^1\Delta$ states in reality. This deficiency might, in principle, deteriorate the quality of these approaches for this particular species, especially of G2 and CBS-Q, since they rely heavily on Møller−Plesset calculations. Schaefer and Xie[19] have studied the $^1\Delta$-$^3\Sigma^-$ energy gap quite carefully. They performed CISD/TZ2P geometry optimizations and vibrational frequency computations for both states. Their energy difference, computed from Figures 1 and 2 of ref 19, is 11.3 kcal/mol at the CISD+Q/TZ2P//CISD/TZ2P+ZPE level. Adding this value to our G2, CBS-Q and G2(QCI) relative energies of $SCC(^3\Sigma^-)+H(^2S)$ one obtains $T = 0$ K reaction energies of 1.2, −1.5 and −0.6 kcal/mol, respectively. We performed MRCISD/cc-pVTZ computations using Schaefer and Xie's geometries, using MCSCF functions as references with an active space $[2\pi,3\pi]$ for six electrons. Our energy $^1\Delta$-$^3\Sigma^-$ energy difference is 10.9 kcal/mol, (the Davidson correction was included). In our opinion, a definitive conclusion on this point could only be reached through very refined treatments of the electron correlation and spin−orbit effects.

We must note that the G2, CBS-Q, and G2(QCI) methods have different merits. The G2(QCI) method can be viewed as an improved G2 method, in which the possible lack of separability of the different contributions to the electronic energy of the latter approach is corrected and also more accurate geometries are employed; the latter feature is probably more important in the present case. It must also be noted that the G2(QCI) method should be expected to behave somewhat better than the G2 method when the reference wave functions present a strong spin contamination, but the CBS-Q method should correct for this deficiency even better, for it has an explicit spin contamination contribution to the electronic energy. In general, the differences between G2 and G2(QCI) results should be

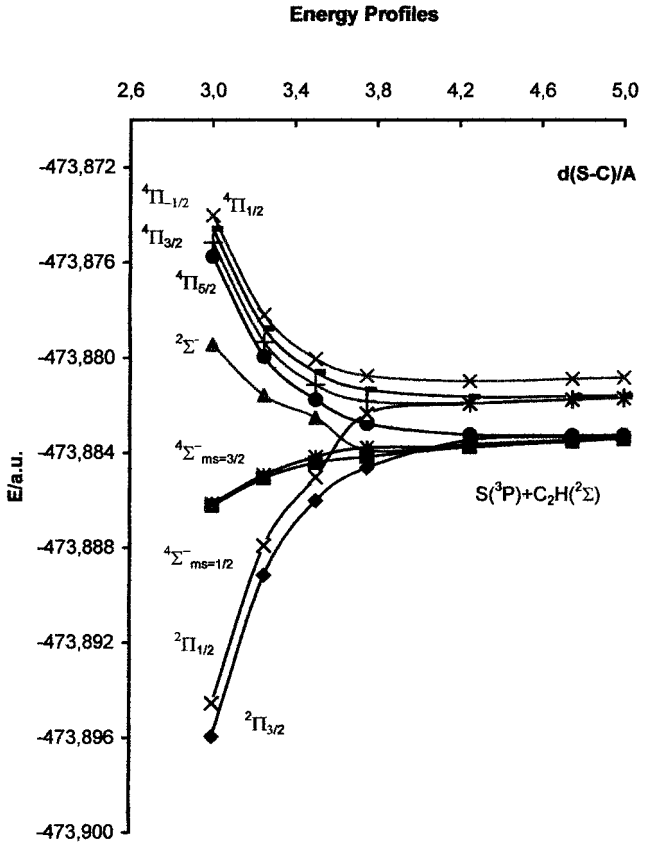

Figure 2. Energy profiles for the electronic states that correlate with S(^{3}P)+C$_2$H($^2\Sigma^+$) for a short range of S−C distances.

attributed mostly to the improved geometries employed in the latter approach, while significant differences between G2 and CBS-Q values should be related to the effects of spin contamination.

Considering the later discussion we would estimate, for instance, that the true reaction energies for the products SCC($^3\Sigma^-$)+H(^{2}S) and SC($^1\Sigma^+$)+CH($^2\Pi$) are probably slightly higher in absolute value than the G2(QCI) values.

IV. The Interaction of S with C_2H

IV.A. Potential Energy Surfaces. The first step in the study of the interaction of S with C_2H was the computation of the $C_{\infty v}$ energy profile in the way we have described above. This energy profile corresponds to the $^2\Pi$ electronic term of SCCH, more precisely, to its $^2B_1$ component in $C_{\infty v}$ symmetry. Recall that the $^2\Pi$ term is the lowest lying and correlates at large $S-C$ distances with S(^{3}P)+C$_2$H($^2\Sigma^+$). The AQCC/aug-cc-pVTZ electronic energies are presented in Table 2.

We also made a study of the evolution of all electronic states that correlate with S(^{3}P,^{1}D)+C$_2$H($^2\Sigma^+$) for large S−C distances in order to establish their repulsive or attractive nature. The corresponding electronic terms (in $C_{\infty v}$ symmetry) are

$$X^2\Pi\ ^4\Pi\ ^4\Sigma\ ^2\Sigma^-\ ^2\Sigma^+\ ^2\Delta\ A^2\Pi$$

We employed an approach that includes the treatment of spin−orbit interactions through the Breit−Pauli Hamiltonian $\hat{H}^{BP}$ (see for instance ref.40); all the computations of this kind were made with the MOLPRO package.[36] The energy shift due to spin−orbit coupling of each state was computed by diagonilazation of the matrix representation of $\hat{H}_{el}+\hat{H}^{BP}$, in which the nondiagonal elements correspond to H^{BP}_{ij}, i and j represent one of the terms mentioned above and $\hat{H}_{el}$ is the electronic Hamiltonian resulting from the Born−Oppenheimer approximation.

TABLE 2: $C_{\infty v}$ Energy Profile for the Interaction of S(^{3}P) with C$_2$H($^2\Sigma^+$) through the $^2\Pi$ State with $\theta = 180^a$

R	E(AQCC)
18.00	−474.102 914 6
16.00	−474.102 914 7
14.00	−474.102 914 9
12.00	−474.102 915 3
10.00	−474.102 916 6
8.00	−474.102 924 9
6.00	−474.102 958 8
5.50	−474.102 990 0
5.00	−474.102 953 5
4.75	−474.103 022 8
4.25	−474.103 346 3
4.00	−474.103 739 1
3.75	−474.104 536 7
3.5	−474.106 362 9
3.25	−474.109 875 0
3.00	−474.117 907 4
2.75	−474.133 222 6
2.5	−474.158 590 8
2.25	−474.193 732 4
2.00	−474.234 404 9
1.85	−474.257 005 6
1.62	−474.273 852 3
1.55	−474.269 868 0

[a] Energies are given in au, the S−C bond distance, R, is given in angstroms.

To determine the nondiagonal matrix elements we employed CI wave functions computed with a common set of orbitals corresponding to a MCSCF wave function optimized for a mixture of all electronic terms, in which they participate with equal weight. In practice, the C_{2v} point group was used to classify all wave functions, not only those needed for the computation of nondiagonal matrix elements. The wave functions assigned to the Σ and Δ states, which may have components belonging to the A_1 and A_2 symmetry species, were optimized subjected to the requirement of producing the right eigenvalue of L_z.

We have introduced some shifts in the spectrum of diagonal matrix elements in an attempt to have more accurate electronic energy differences between terms. In this respect, it is worth recalling that the MCSCF method is deficient in the sense that the dynamical electron correlation effects are, at the most, only partly included. We determined these energy shifts in the following ways:

(i) For the lowest term of each symmetry and spin multiplicity, we made a MRCI computation using a reference wave function of the CASSCF type optimized for this particular term.

(ii) If there is another term of the same spin and symmetry, the energy difference with respect to the lower lying counterpart is given by the gap between the lowest two roots in a CASSCF computation for an equal mixture of both terms.

In all cases a valence double-ζ basis set including a shell of d-functions in sulfur was employed. The active space of the CASSCF wave functions is [$9a_1 10a_1 3b_1 3b_2$], which would have the following description for large S−C distances: [3σ(C$_2$H) 3p$_z$(S) 3p$_x$(S) 3p$_y$(S)].

Figure 2 presents the *diabatic* energy profiles for all the levels that correlate with S(^{3}P)+C$_2$H($^2\Sigma^+$) in a short range of S−C distances, where the chemical interactions become important. These curves are drawn without taking into account the avoided crossings caused by the spin−orbit interactions. It is readily seen that only the levels arising from the $X^2\Pi$ term are truly attractive. It is interesting that $^2\Pi_{1/2}$ correlates with S(^{3}P$_1$) and

crosses up to four other levels; this means that the adiabatic curves would form a complex set of avoided crossings. Note that there is a particularly strong $^2\Pi_{1/2}$-$^2\Sigma^-$ interaction, which has a noticeable effect in the shape of the corresponding diabatic surfaces. There is a conspicuous avoided crossing; a reactive trajectory of a system evolving on the upper $^2\Pi_{1/2}$−$^2\Sigma^-$ adiabatic surface should undergo a nonadiabatic transition into its lower counterpart, which corresponds to a pure $^2\Pi_{1/2}$ state at short range.

IV.B. Long-Range Potential. We have modeled the potential surfaces corresponding to the $^2\Pi_{3/2}$ and $^2\Pi_{1/2}$ levels by combining short and long-range potentials through the following procedure.

The long-range potential is derived from the expressions corresponding to the electrostatic, induction and dispersion interactions obtained by Buckingham[41] through perturbation theory, taking into account the tensorial nature of the molecular polarizabilities, the quadrupoles, and higher moments. Specifically, we used the expressions corresponding to the interaction of linear molecules,[41] adequately simplified for our case. We will distinguish three parts, namely, induction, dispersion, and electrostatic:

$$V_{\text{ind}} = -\frac{1}{2}\alpha_2\mu_1^2(3\cos^2\theta + 1)/r^6 - 6\alpha_2\mu_1\Theta_1\cos^3\theta/r^7$$

$$V_{\text{dis}} = -[3U_1U_2\alpha_2/2(U_1 + U_2)r^6]\Big\{\alpha_1 + \frac{1}{6}(\alpha_{1,\|} - \alpha_{1,\perp})(3\cos^2\theta - 1) + 2A_{1\|}\cos^3\theta/r + \frac{4}{3}A_{1\perp}(3\cos\theta - 2\cos^3\theta)/r\Big\}$$

$$V_{\text{el}} = \frac{3}{2}\mu_1\Theta_2(\theta)f(\cos(\theta))/r^4 \qquad (1)$$

The indexes 1 and 2 refer to C_2H and S, respectively; $f(\cos(\theta))$ is a function of the angle which will be specified later. The variable r is the distance between the centers of mass and θ is the angle between the molecular dipole and the line connecting the centers of masses. μ, Θ, and α represent the dipole and quadrupole moments and the polarizabilities; $\alpha_\|$ and $\alpha_\perp$ represent the polarizabilities corresponding to the symmetry axis and the direction perpendicular to it, respectively. $A_{1\|}$, $A_{1\perp}$, and $U_{12}=U_1U_2/(U_1 + U_2)$, were determined by a fitting procedure to be described later.

The dipole and polarizability anisotropy of sulfur are zero. The quadrupole moment of the isolated atom must be zero as well, but the electrostatic field exerted by the CCH group causes some degree of anisotropy; since we found this effect is not negligible, it was treated as an adjustable parameter. In a configuration interaction picture of the electron density, one can explain the anisotropy as an imbalance in the weights of electronic configurations that are degenerate for the isolated atom. These configurations produce different values of the quadrupole components, but in such a way that the resultant is zero when they have equal weights. In fact, the same reasoning would apply to the polarizability anisotropy of sulfur; the terms of the induction potential in which it would appear have a r^{-6} dependence, as the main terms of the induction and dispersion potentials written above. It turns out that the fitting process giving values for the adjustable parameters of the latter potential cannot be made fine enough to include an additional r^{-6} dependent term; its effect will be basically absorbed in the dispersion potential.

To determine the adjustable parameters we did the following:

(i) First we took the outer part of the AQCC/aug-cc-pVTZ energy profile (d(S−C)≥8 Å), corrected it for basis set superposition error (BSSE), and fit to it $V_{\text{ind}} + V_{\text{dis}}$, in which only U_{12} and $A_{1\|}$ were taken as adjustable parameters. We employed $A_{1\perp} = -A_{1\|}/2$; this approximation implies the neglect of the $r^{-7}P_1(\cos\theta)$ term in the expression of V_{dis}.[41] The BSSE was determined through the counterpoise method;[42] single-configuration wave functions were employed as reference in the AQCC computations of the fragments. The values of dipole and quadrupole moments were determined as expectation values of single-reference AQCC/aug-cc-pVTZ wave functions whereas the polarizabilities were determined as numerical second derivatives, at the same level. We employed the asymptotic geometry of the C_2H group obtained in the reaction coordinate.

(ii) To determine the behavior of the quadrupole moment of sulfur, we performed AQCC/cc-pVTZ computations for several values of r and two values of θ, namely 0 and π, and corrected for BSSE. The reference functions in the AQCC computations were of the same type employed in the determination of the energy profile. Note that the energy difference of the two angular conformations is a function of the terms containing odd powers of $\cos\theta$. It turns out that the r dependence of the energy difference is, quite neatly, r^{-4}; this result only means that the electrostatic term is the most important. However, when one examines the r dependence of the energy profile one encounters a leading power of −6. Since the depth of the potential $E(r,\theta=\pi) - E(\infty,\theta=\pi)$ is comparable to its anisotropy for large r, this implies that $\Theta_2(\theta_1=\pi) \approx 0$.

The strength of the electrostatic term prevented any reliable determination of the ratio $A_{1\perp}/A_{1\|}$, which, in principle, could have been deduced from the anisotropy of the potential, so we took as definitive the value $-1/2$ employed in the first step. Finally, we used an expression for the electrostatic energy which includes an effective quadrupole, the angular dependency is given only by $1 - \cos\theta$. The effective atomic quadrupole is determined through the average

$$\Theta_2 = \langle r^4[E(r,\theta=0) - E(r,\theta=\pi)]\rangle/3\mu_1 \qquad (2)$$

which was computed for values of r, such $8 < r < 18$ Å. The present treatment appears to reproduce quite well the anisotropy of the ab initio potential so we did not pursue any further improvements.

Having determined the adjustable parameters we defined the *long-range* part of the potential as $V_{\text{lr}} = V_{\text{ind}} + V_{\text{dis}} + V_{\text{ele}}$. The only modification is that the values given to $\{\mu_1,\Theta_1,\alpha_1, \alpha_{1,\|}-\alpha_{1,\perp}\}$ were computed at the B3LYP/aug-cc-pVQZ level and α_2 is given the experimental value.[43] The success of the B3LYP method in the computation of the electric properties has already been established.[44]

For the short-range part we used a stiff Morse potential to account for the r dependence.[45] The angular dependence was modeled by means of the following expression:

$$V_d(R,\chi) = Ae^{-(\eta_0+\eta_1 R+\eta_2 R^2)R}(1 - \cos\chi) \qquad (3)$$

where χ is the ∠SCC angle and R is the S−C distance. The parameters of V_{m} were determined by a Levenberg−Marquardt method by fitting to points of the energy profile such that $R <$ 4 Å. We performed CASSCF/cc-pVDZ computations for a set of (R,χ) data for both the $^2A'$ and $^2A''$ states (that correlate with

TABLE 3: Corrections to the Long-range Potential Given in hartree

R/Å	$-E_{BSSE}(\theta=0)^a$	$E(\theta=0) - E(\theta=\pi)^b$	$E_{BSSE}(\theta=\pi) - E_{BSSE}(\theta=0)^b$	$E_{so}(^2\Pi_{3/2})$	$E_{so}(^2\Pi_{1/2})$
12.0	$<10^{-7}$	0.000 006	$<10^{-7}$	−0.000 853	0.000 838
10.0	0.000 004	0.000 012	$<10^{-7}$	−0.000 853	0.000 838
8.0	0.000 006	0.000 036	$<10^{-7}$	−0.000 853	0.000 836
6.0	0.000 022	0.000 082	0.000 005	−0.000 865	0.000 817
5.5	0.000 034	0.000 113	0.000 008	−0.000 876	0.000 811
5.0	0.000 059	0.000 170	0.000 015	−0.000 837	0.000 761
4.75	0.000 076	0.000 229	0.000 020	−0.000 823	0.000 748
4.25	0.000 122	0.000 571	0.000 027	−0.000 700	0.000 829
3.5	0.000 236	0.004 226	0.000 098	−0.000 773	0.001 047

[a] Computed at the AQCC/aug-cc-pVTZ level. [b] Computed at the AQCC/cc-pVTZ level and corrected for BSSE.

the $^2\Pi$ term of linear geometries) and determined the parameters of V_d for each state.

Before assembling the total potential with long and short-range parts, it is convenient to introduce spin−orbit corrections in order to improve accuracy and be able to distinguish between the two levels of the of the $^2\Pi$ term. We have two corrections for each point of the reaction coordinate, namely, $\Delta E_{so}[^2\Pi_{3/2},^2\Pi_{1/2}](R)$. The effect of the spin−orbit correction on the short range potential is taken into account simply by shifting the dissociation energy:

$$D_e(^2\Pi_\Omega) = D_e - E_{so}(^2\Pi_\Omega)(R=R_e) + E_{so}(^2\Pi_\Omega)(R\rightarrow\infty) \quad (4)$$

Besides, the long-range potential is modified by adding the following correction:

$$\Delta E_{so,lr}(^2\Pi_\Omega)(r) = E_{so}(^2\Pi_\Omega)(r) - E_{so}(^2\Pi_\Omega)(r\rightarrow\infty) \quad (5)$$

In the present case the r dependence of the long-range part of the spin−orbit correction is adequately represented by a power series of the type:

$$E_{so,lr}(r) = E_{so}(r\rightarrow\infty) + A_{so}/r^8 + B_{so}/r^{10} \quad (6)$$

In the case of the $^2\Pi_{1/2}$ level, the spin−orbit corrections correspond to the diabatic curve, their use leading to a diabatic energy profile.

The total potential is constructed with short and long-range parts, combining them by means of the switching function $w(R)$ defined in reference,[46] in the following way:

$$V = (V_m + V_d)w + (V_{lr} + \Delta E_{so,lr})(1 - w) \quad (7)$$

Note we will have four potentials, for we have two different levels for linear geometries that correlate with $^2A'$ and $^2A''$ states of planar C_s geometries. Note also that the angle dependent part of the long-range potential is independent of the C_s state considered; i.e., it is the same for the $^2A'$ and $^2A''$ states.

The corrections to the long-range potential are presented in Table 3.

V. Approximate Classical Trajectory Computations

As stated above, we have made a study of the reaction dynamics of the capture step for the lowest lying levels $^2\Pi_{3/2},^2\Pi_{1/2}$. We employed the following Hamiltonian for the long-range region:

$$H_{lr} = \frac{p_r^2}{2\mu} + V_{min}(r) + \frac{|\vec{J} - \vec{j}|^2}{2\mu r^2} + \frac{p_\theta^2}{2I} + \frac{(p_\phi - p_\psi\cos\theta)^2}{2Isin^2\theta} + \frac{p_\psi^2}{2I_3} + V_0(r,\theta) \quad (8)$$

The vectors $\vec{J}$ and $\vec{j}$ represent the total collision and rotation angular momentum. $V_{min}(r)$ represents the minimum of the long-range potential for a particular value of r, the distance between the centers of mass, and $V_o(r,\theta)$ represents the orientation potential. The total potential would be, of course, $V(r,\theta) = V_{min}(r) + V_o(r,\theta)$. Recall that θ represents the angle of the dipole moment with respect to the line connecting the centers of mass. I is the moment of inertia, μ is the reduced mass of the collision, and p_r is the momentum associated with the coordinate r. The other momenta correspond to the rotations of C_2H and have the following expressions:

$$p_\psi = I_3(\dot{\phi}\cos\theta + \dot{\psi})$$

$$p_\phi = (I\sin^2\theta + I_3\cos^2\theta)\dot{\phi} + I_3\dot{\psi}\cos\theta$$

$$p_\phi = I\dot{\theta} \quad (9)$$

The momentum p_ψ would classically represent the rotation of a molecule, in this case the C_2H group, with respect to its symmetry axis; in our case it will be invariant and made equal to $\Omega\hbar$. Given that the ground state of C_2H is $(^2\Sigma^+)$ this momentum is finally zero. Besides, in the long-range region, the projection of the rotational angular momentum on the line connecting the centers of masses is given by the quantum number M; consequently the rotational part of the Hamiltonian reduces to

$$H_r = \frac{p_\theta^2}{2I} + \frac{M^2\hbar^2}{2I\sin^2\theta} + V_0(r,\theta) \quad (10)$$

The second term of the right-hand side can be viewed as a θ-dependent effective potential. This Hamiltonian is singular for $\theta = 0$ or $\theta = \pi$; but these values are never reached for $M \neq 0$ (see below, eq 12).

Each trajectory has a particular set of quantum numbers, $\{J,j,M\}$, as well as a particular energy E. The values of j and M are sampled. Each trajectory is also given values of the relative speed g and the impact parameter b; the orbital angular momentum is then determined by $l = \mu g b$, as well as the total energy. All possible couplings of rotational and orbital angular momenta are considered through the particular value of $J = \{|l-j|, .., l+j\}$; J is considered a real number in practice. We made the approximation of ignoring the coupling between rotational and spin angular momenta, which is not expected to produce an important error, for taking it into account would almost simply imply shifting up and down j by $^1/_2$. The spin-rotation coupling constant is very small compared to the rotational constant in this case.[47] We also chose to consider both J and j good quantum numbers; the corresponding term in the Hamiltonian is then written as follows:

$$\frac{|\vec{J}-\vec{j}|^2}{2\mu r^2}=\frac{\hbar^2}{2\mu r^2}[J(J+1)-2M^2+j(j+1)] \quad (11)$$

Note this choice is consistent with the centrifugal sudden approximation.[48]

One also needs initial values of θ; we chose a random number limited by the roots of the following equation:

$$\dot{s}^2=(1-s^2)\left[(E_r-V_o(r_0,\theta))\frac{2}{I}\right]-\left(\frac{\hbar}{I}\right)^2(M-s\Omega)^2; \quad s=\cos(\theta) \quad (12)$$

sampling a normalized probability $\sin\theta$, where r_0 is the initial value of the distance between centers of mass and E_r is the rotational energy, excluding the component to the rotation about the symmetry axis if present. Note that the present treatment differs from Choi and Bernstein's theory of oriented symmetric-top molecular beams[49] in the fact that the magnitude and functional form of the orientation potential have also a direct influence in the range of allowed values of θ: it is not determined solely by the rotational quantum numbers. The orientations are weighted by $\sin\theta$; although this procedure is not optimal, we have checked that the angular sampling was fine enough for reaching convergence.

The end of the long-range region depends on the trajectory, and is reached when eq 12 has fewer than two real roots with absolute value lower than one. This situation is that of a locked dipole. At this point, we switch to a second model, the corresponding Hamiltonian being given basically by an expression similar to (10) but in which p_ϕ is not determined by the quantum number M. Since our potential is independent of ϕ even at short range, the second term is simply replaced by a constant $M^2\hbar^2/2I \sin^2\theta_c$, where θ_c is the value of θ at which we change model. The centrifugal potential is now approximated simply as

$$\frac{|\vec{J}-\vec{j}|^2}{2\mu r^2}\approx\frac{\hbar^2}{2\mu r^2}J(J+1) \quad (13)$$

and the radial speed is adjusted to maintain a constant energy.

A particular trajectory is considered reactive if it reaches a point where the S−C distance is less than 1.3 R_e. We will show below that the degree of dissociation of $SCCH(^2\Pi)$ into the reactants computed by RRKM theory is rather low.

We would like to stress that the present method emphasizes the adequate treatment of the angular momentum as well as the use of accurate long-range PES for the attractive spin−orbit levels; these are the decisive factors. It would be possible, in principle, to perform full trajectory computations using all the coordinates, but then one would face the very difficult task of the PES parametrization for several spin−orbit levels.

VI. Results of the Trajectory Computations

We made some approximate classical trajectory computations for the levels with attractive energy profiles: $^2\Pi_{3/2}$ and $^2\Pi_{1/2}$. In both cases we made them correlate with the $^2A'$ component for nonlinear planar geometries at short range; i.e., the expression given to V_d of eq 3 is the one corresponding to the $^2A'$ state. However, we found that the rate coefficients are quite insensitive to the choice of V_d.

We must recall that, in the case of the $^2\Pi_{1/2}$ level, the potential surface is built from a diabatic energy profile; this choice is almost equivalent to admitting that the probabilities of nonadiabatic transition at the crossing points are 1. In other words, the rate coefficients for this level should be viewed as upper limits. We also give total or combined rate coefficients computed using the following expression:

$$k_T=k(^2\Pi_{3/2})_T f(^3P_2)_T+k(^2\Pi_{1/2})_T f(^3P_1)_T \quad (14)$$

We have assumed a thermal distribution between levels in the long-range region; these levels correspond to the $^3P_2$, $^3P_1$, and $^3P_0$ levels of sulfur. It is also assumed that a transition into the attractive level of each set will take place, through Rosen−Zener−Demkov coupling in the case of the $^2\Pi_{1/2}$ level, and also through Landau−Zener coupling in the case of the $^2\Pi_{3/2}$ level, given that it crosses the other levels that correlate with $S(^3P_2)+C_2H(^2\Sigma^+)$ (see Figure 2). See, for instance, ref. 50 for a review of nonadiabatic transitions. In other words, all the levels that correlate with $S(^3P_2)+C_2H(^2\Sigma^+)$ contribute to $k(^2\Pi_{3/2})_T$ while those connecting with $S(^3P_1)+C_2H(^2\Sigma^+)$ contribute to $k(^2\Pi_{1/2})_T$; $S(^3P_0)$ and $C_2H(^2\Sigma^+)$ would not react. These transitions would take place in a range of S−C distances where the PES of the levels having a common dissociation limit lie still quite close. Under this assumption it is fair to use the PES of the $^2\Pi_{3/2}$ and $^2\Pi_{1/2}$ levels as representative of all the levels connecting with $S(^3P_2)+C_2H(^2\Sigma^+)$ and $S(^3P_1)+C_2H(^2\Sigma^+)$, respectively.

The functions f are just statistical weight functions. It could happen that the distribution between the lowest levels of sulfur is not thermal; in such a case the total rate could be recomputed using alternative f functions and the data of Table 4.

Under all these assumptions, it is obvious that the combined rate coefficients must be considered upper bounds of the rates of reaction corresponding to the reactants in a thermal energy distribution.

It is readily seen in Table 4 that the two levels considered provide very different reaction rates, the ones corresponding to $^2\Pi_{3/2}$ being much higher. The reason is that the PES of the $^2\Pi_{1/2}$ level is less attractive; there is even a maximum in the $\theta=\pi$ energy profile, which lies slightly above the reactants, about 0.35 kJ/mol higher. The contribution of the $^2\Pi_{1/2}$ level to the combined rate is rather small, only about 9% at $T=300$K, due mostly to the sizable energy gap between $S(^3P_2)$ and $S(^3P_1)$. This contribution diminishes to 0.01% at $T=60$ K; but this effect is not sufficient to balance the significant decrease of the rate coefficients of both levels.

Even though its rate at $T=300$ K is quite high for a neutral−neutral reaction, it would hardly be higher than that of most

TABLE 4: Rate Coefficients (in Units of 10^{-10} cm^3 s^{-1})[a]

T/K	$k(^2\Pi_{3/2})$	$k(^2\Pi_{1/2})$	k
40	2.31	0.11	2.31
60	2.57	0.27	2.57
80	2.70	0.24	2.70
100	2.97	0.43	2.97
200	3.42	0.76	3.29
300	3.66	1.05	3.32
400	3.84	1.30	3.41
500	3.99	1.55	3.46

[a] Potential energy parameters: (D_e(J/mol) = 449948, $\beta_0=1.55$ Å^{-1}, $\beta_1=0.13$ Å^{-2}, $R_e=1.63447$ Å, for the stiff-Morse potential), α'_2(S) = 2.90 Å^3, $\Theta_2=2.87$ D Å, $\mu_1=0.7727$ D, $\alpha'_1=3.77$ Å^3, $\alpha_{1,\parallel}'$ - $\alpha_{1,\perp}'$ = 0.415 Å^3, $A_{1\perp}=-0.2175\times10^{-6}$ F m,[4] $U_{12}=44720$ cm^{-1}, $\Theta_1=4.58$ D Å. For the $^2A'$ state: $A=8.2980\times10^6$ J/mol, $\eta_0=13.18$ Å^{-1}, $\eta_1=-5.502$ Å^{-2}, $\eta_2=0.8268$ Å^{-3}, for the $^2A''$ state: $A=4.051\times10^6$ J/mol, $\eta_0=11.81$ Å^{-1}, $\eta_1=-4.840$ Å^{-2}, $\eta_2=0.7372$ Å^{-3}. For the $^2\Pi_{3/2}$ state: $A_{so}=-19.54$ hartree Å.[8] For the $^2\Pi_{1/2}$ state: $A_{so}=-172.58$ hartree Å,[8] $B_{so}=9265.025$ hartree Å.[10] The parameters of the switching function are $\gamma=5.0$ Å^2, $b=1.9$ Å^{-1}, $R_c=4.25$ Å. Rotational constant of $C_2H(^2\Sigma^+)$: 1.4750 cm^{-1}.

ion−molecule reactions at low temperatures. Particularly, the reaction $S^+ + C_2H_2 \rightarrow SC_2H^+ + H$ was found by experiment to have a rate coefficient[23] of $k = 9.8 \times 10^{-10}$ cm^3 s^{-1}, which must be expected to increase with decreasing temperature; (in fact our preliminary computations indicate that the k(60 K)/k(300 K) ratio should be about 1.6). However, to produce SC_2 from SC_2H^+ it is necessary to have a dissociative recombination step; its efficiency and the identity of the products are not known. Recall that, according to Table 1, our reaction is exothermic by only about 10 kcal/mol. Finally, the contribution of both reactions to the production of SC_2 will ultimately depend on the abundances and the degree of overlap of the reactants.

VII. A Preliminary Study of the Evolution of the SC_2H Complex

A preliminary study of the evolution of the SC_2H complex formed in the collision has been carried out, by combining the study of the reaction intermediates and saddle points with RRKM-type computations. Although using other types of methods would be convenient for obtaining definitive conclusions, the present approach should be sufficient for a semiquantitative discussion, given that our PES has rather deep minima. The most important aspect of the present study is the use of a distribution function for the population of total energy and angular momentum that corresponds to the reactive collisions, instead of the thermal distribution. See refs 51 and 46 and the refs cited therein for details and a general discussion of RRKM theory. We used G2(QCI) relative energies, QCISD/6-311++G** geometries, and MP2=full/6-31G* vibrational frequencies.

We have assumed that most of the reactive collisions will generate SCCH($^2\Pi$). Given that the transition state TS12($^2A''$) which connects this species with SC_2H($^2A''$) is quite low in energy one would expect SCCH($^2\Pi$) to rearrange immediately into the latter state. The dissociation of SCCH($^2\Pi$) into the reactants has a rate coefficient $k_1 = 0.019$ ps^{-1} at $T = 300$ K; there is a significant reduction with decreasing temperature ($k_1 = 0.0009$ ps^{-1} at $T = 60$ K). The rate coefficients for the isomerization process are indeed much higher; their values are $k_2 = 4.1$ and 3.8 ps^{-1} for $T = 300$ K and $T = 60$ K, respectively.

SC_2H($^2A''$) may rearrange into HSCC($^2A''$); the rate coefficients for this process are 0.90 ps^{-1} and 0.74 ps^{-1} at $T = 300$ K and $T = 60$ K, respectively. These rates are somewhat lower than those of the isomerization back into SCCH($^2\Pi$) (4.7 ps^{-1} and 4.5 ps^{-1} for $T = 300$ K and $T = 60$ K respectively). The rate coefficients for the dissociation of HSCC($^2A''$) into SCC($^3\Sigma^-$)+H(^{2}S) are 0.44 ps^{-1} and 0.15 ps^{-1} at $T = 300$K and $T = 60$ K, respectively. Note that these values are more than one order of magnitude higher than the ones corresponding to the fragmentation of SCCH($^2\Pi$) into the reactants.

SCHC($^2A'$) is such a shallow minimum that it is better to consider the generation of SCC($^1\Delta$)+H(^{2}S) from SCCH($^2\Pi$) as a one-step process from a dynamical point of view; the minimum being just one point on the reaction coordinate. We computed an approximate reaction coordinate connecting SCHC($^2A'$) with SCC($^1\Delta$)+H(^{2}S) by means of partial geometry optimizations for a series of C−H distances, while keeping constant ∠CCH = 90°. These computations were performed at the B3LYP/6-31G** level. Although this is a rather poor description of the process, we feel it should be sufficient to give a rough estimate of the rate coefficients; our results are 0.02 ps^{-1} ($T = 300$ K) and 0.0001 ps^{-1} at ($T = 60$ K). At this point we must recall that the $^2A'$ and $^2A''$ electronic states are quite close in energy for geometries in vicinity of the SCHC($^2A'$) minimum, and mix significantly if the geometry is allowed to be nonplanar and the C−H bond is stretched. This implies that if the system evolves on the $^2A'$ surface it may still derive SCC($^3\Sigma^-$)+H(^{2}S) through nonplanar geometries. This process is likely to have a rate higher than the one computed for the production of SCC($^1\Delta$)+H(^{2}S), given the $^1\Delta$-$^3\Sigma^-$ energy gap.

Our computations indicate that the fragmentation of the complex into the reactants causes a reduction of only about 3% ($T = 300$ K) and (0.25%) ($T = 60$ K) of the reaction rate with respect to the capture values. An improved RRKM-type treatment, including all possible processes, should probably give even smaller reductions.

VIII. Conclusions

We have made a theoretical study of the S + C_2H reaction. In the study of the PES of the SC_2H system four minima were found, namely, in increasing energy order: SCCH($^2\Pi$), SC_2H-($^2A''$), HSCC($^2A''$) and SCHC($^2A'$). The first species is a relatively deep minimum lying about 114 kcal/mol below the reactants.

We have analyzed the interaction of S(^{3}P) and S(^{1}D) with C_2H($^2\Sigma^+$), including spin−orbit interactions, as a first step to a rather detailed modeling of the PES for the interaction through the $^2\Pi_{3/2}$ and $^2\Pi_{1/2}$ levels; the only ones that present an attractive energy profile. Using the resulting PES we performed classical trajectory computations in order to estimate upper bounds to the reaction rates. It turns out that the reaction is quite fast if occurring through the $^2\Pi_{3/2}$ PES, whereas it is rather slow if it takes place through the $^2\Pi_{1/2}$ PES. However, the contribution of the latter term to the total reaction rate should be quite small if the sulfur atoms present a thermal distribution among the levels of the ^{3}P term. The total reaction rate is found to decrease with temperature, but not too sharply.

The main product should be SCC($^3\Sigma^-$)+H(^{2}S), and must be generated mainly by evolution of the SC_2H complex on the $^2A''$ PES, although the $^2A'$ state might also play a role.

Concerning the implications of the present study in molecular astrophysics, we must note that the reaction of S^+ with acetylene, which is thought to be the first step in the production of SC_2 from sulfur cations, has a much higher rate coefficient for low temperatures. However, the present reaction is still rather fast and could also be a direct an efficient way of generating SC_2.

Acknowledgment. We are glad to acknowledge financial support from government of the autonomous community of Galicia (Projects PGIDT99PXI30102B and PGIDT00PXI-30104PN) and the Spanish ministry of education (Project PB98-1085). J.R.F. thanks Prof. T. J. Millar for some helpful discussions.

References and Notes

(1) Smith, D. *Chem. Rev.* **1992**, *92*, 1473.
(2) Herbst, E. *Annu. Rev. Phys. Chem.* **1995**, *46*, 27.
(3) Suzuki, H.; Kaifu, N.; Miyaji, T.; Morimoto, M.; Ohishi, M.; Saito, S. *Astrophys. J.* **1984**, *282*, 197.
(4) Saito, S.; Kawaguchi, K.; Yamamoto, S.; Ohishi, M.; Suzuki, H.; Kaifu, N. *Astrophys. J. Lett.* **1987**, *317*, L115.
(5) Yamamoto, S.; Saito, S.; Kawaguchi, K.; Kaifu, N.; Suzuki, H.; Ohishi, M. *Astrophys. J. Lett.* **1987**, *317*, L119.
(6) Cernicharo, J.; Guélin, M.; Hein, H.; Kahane, C. *Astron. Astrophys.* **1987**, *181*, L9.
(7) Bell, M. B.; Avery, L. W.; Feldman, P. A. *Astrophys. J.* **1993**, *417*, L37.
(8) Szczepanski, J.; Hodyss, R.; Fuller, J.; Vala, M. *J. Phys. Chem.* **1993**, *103*, 1975.

(9) Maier, G.; Reisenauer, H. P.; Schrot, J.; Janoschek, R. *Angew. Chem., Int. Ed. Engl.* **1990**, *29*, 1464.
(10) Lovas, F. J.; Suenram, R. D.; Ogata, T.; Yamamoto, S. *Astrophys. J.* **1992**, *399*, 325.
(11) Ohshima, Y.; Endo, Y. *J. Mol. Spectrosc.* **1992**, *153*, 627.
(12) Hirahara, Y.; Ohshima, Y.; Endo, Y. *Astrophys. J.* **1993**, *408*, L113.
(13) Kasai, Y.; Obi, K.; Ohshima, Y.; Hiahara, Y.; Endo, Y.; Kawaguchi, K.; Murakami, A. *Astrophys. J.* **1993**, *410*, L45.
(14) Krishnamachari, S. L. N. G.; Ramsay, D. A. *J. Chem. Soc., Faraday. Discuss.* **1981**, *71*, 205.
(15) Coquart, B. *Can. J. Phys.* **1985**, *63*, 1362.
(16) Dunlop, J. R.; Karolczak, J.; Clouthier, D. J. *Chem. Phys. Lett.* **1988**, *151*. 362.
(17) Vrtilek, J. M.; Gottlieb, C. A.; Gottlieb, E. W.; Wang, W.; Thaddeus, P. *Astrophys. J.* **1992**, *L73*, 398.
(18) Lee, S. *Chem. Phys. Lett.* **1997**, *268*, 69.
(19) Xie, Y.; Schaefer, H. F., III *J. Chem. Phys.* **1992**, *96*, 3714.
(20) Li, Y.; Iwata, S. *Chem. Phys. Lett.* **1997**, *273*, 91.
(21) Szalay, P. G.; Blaudeau, J.-P. *J. Chem. Phys.* **1997**, *106*, 436.
(22) Szalay, P. G. *J. Chem. Phys.* **1996**, *105*, 2735.
(23) Smith, D.; Adams, N. G.; Giles, K.; Herbst, E. *Astron. Astrophys.* **1988**, *200*, 191.
(24) Willacy, K.; Millar, T. J. *Astron. Astrophys.* **1997**, *324*, 237.
(25) Petrie, S. *Mont. Not. R. Astron. Soc.* **1996**, *281*, 666.
(26) Herbst, E.; Woon, D. E. *Astrophys. J.* **1997**, *489*, 109.
(27) Woon, D. E.; Herbst, E. *Astrophys. J.* **1997**, *477*, 204.
(28) Curtiss, L. A.; Raghavachari, K.; Trucks, G. W.; Pople, J. A. *J. Chem. Phys.* **1991**, *94*, 7221.
(29) Ochterski, J. W.; Petersson, G. A.; Montgomery,, J. A., Jr. *J. Chem. Phys.* **1996**, *104*, 2598.
(30) Pople, J. A.; Head-Gordon, M.; Raghavachari, K. *J. Chem. Phys.* **1987**, *87*, 5968.
(31) Durant, J. L., Jr.; McMichael Rohlfing, C. *J. Chem. Phys.* **1991**, *98*, 8031.
(32) Szalay, P. G.; Bartlett, R. J. *Chem. Phys. Lett.* **1993**, *214*, 481.
(33) Gdanitz, R. L.; Ahlrichs, R. *Chem. Phys. Lett.* **1988**, *143*, 413.
(34) Woon, D. E.; Dunning, T. H., Jr. *J. Chem. Phys.* **1993**, *98*, 1358.
(35) Shepard, R.; Shavitt, I.; Pitzer, R. M.; Comeau, D. C.; Pepper, M.; Lischka, H.; Szalay, P.; Ahlrichs, R.; Brown, F. B.; Zhao, J. G. *Int. J. Quantum. Chem: Quantum. Chem. Symp.* **1988**, *22*, 149.
(36) Werner, H.-J.; Knowles, P. J.; Amos, R. D.; Bernhardsson, A.; Berning, A.; Celani, P.; Cooper, D. L.; Deegan, M. J. O.; Dobbyn, A. J.; Eckert, F.; Hampel, C.; Hetzer, G.; Korona, T.; Lindh, R.; Lloyd, A. W.; McNicholas, S. J.; Manby, F. R.; Meyer, W.; Mura, M. E.; Nicklass, A.; Palmieri, P.; Pitzer, R.; Rauhut, G.; Schütz, M.; Stoll, H.; Stone, A. J.; Tarroni, R.; Thorsteinsson. T. MOLPRO (http://www.tc.bham.ac.uk/molpro).
(37) Frisch, M. J.; Trucks, G. W.; Schlegel, H. B.; Gill, P. M. W.; Johnson, B. G.; Robb, M. A.; Cheeseman, J. R.; Keith, T.; Petersson, G. A.; Montgomery, J. A.; Raghavachari, K.; Al-Laham, M. A.; Zakrzewski, V. G.; Ortiz, J. V.; Foresman, J. B.; Cioslowski, J.; Stefanov, B. B.; Nanayakkara, A.; Challacombe, M.; Peng, C. Y.; Ayala, P. Y.; Chen, W.; Wong, M. W.; Andres, J. L.; Replogle, E. S.; Gomperts, R.; Martin, R. L.; Fox, D. J.; Binkley, J. S.; Defrees, D. J.; Baker, J.; Stewart, J. P.; Head-Gordon, M.; Gonzalez, C.; Pople, J. A. *Gaussian 94*; Gaussian, Inc.: Pittsburgh, PA, 1995.
(38) Frisch, M. J.; Trucks, G. W.; Schlegel, H. B.; Scuseria, G. E.; Robb, M. A.; Cheeseman, J. R.; Zakrzewski, V. G.; Montgomery, J. A., Jr.; Stratmann, R. E.; Burant, J. C.; Dapprich, S.; Millam, J. M.; Daniels, A. D.; Kudin, K. N.; Strain, M. C.; Farkas, O.; Tomasi, J.; Barone, V.; Cossi, M.; Cammi, R.; Mennucci, B.; Pomelli, C.; Adamo, C.; Clifford, S.; Ochterski, J.; Petersson, G. A.; Ayala, P. Y.; Cui, Q.; Morokuma, K.; Malick, D. K.; Rabuck, A. D.; Raghavachari, K.; Foresman, J. B.; Cioslowski, J.; Ortiz, J. V.; Stefanov, B. B.; Liu, G.; Liashenko, A.; Piskorz, P.; Komaromi, I.; Gomperts, R.; Martin, R. L.; Fox, D. J.; Keith, T.; Al-Laham, M. A.; Peng, C. Y.; Nanayakkara, A.; Gonzalez, C.; Challacombe, M.; Gill, P. M. W.; Johnson, B. G.; Chen, W.; Wong, M. W.; Andres, J. L.; Head-Gordon, M.; Replogle, E. S.; Pople, J. A. *Gaussian 98*; Gaussian, Inc.: Pittsburgh, PA, 1998.
(39) Brunck, T. K.; Weinhold, F. *J. Am. Chem. Soc.* **1978**, *102*, 1700. (b) Foster, J. P.; Weinhold, F. *J. Am. Chem. Soc.* **1980**, *102*, 7211. (c) Reed, A. E.; Weinhold, F. *J. Chem. Phys.* **1985**, *83*, 1736. (d) Reed, A. E.; Weinstock, R. B.; Weinhold, F. *J. Chem. Phys.* **1985**, *83*, 735. (e) Reed, A. E.; Curtiss, L. A.; Weinhold, F. *Chem. Rev.* **1988**, *88*, 899. (f) Weinhold, F. A. In *Encyclopedia of Computational Chemistry*; Schleyer, P. V. R., Ed.; John Wiley & Sons Ltd. Publishers: New York, 1998; Vol. 3, pp 1792−1810. (g) NBO 4.M. Glendening, E. D.; Badenhoop, J. K.; Reed, A. E.; Carpenter, J. E.; Weinhold, F.; Theoretical Chemistry Institute, University of Wisconsin: Madison, 1999.
(40) Hess, B. A.; Marian, C. M.; Peyerimhoff, S. D. In *Modern Electronic Structure Theory*; Yarkony, D. R., Ed.; World Scientific: River Edge, NJ, 1995; Part I, Chapter 4.
(41) Buckingham, A. D. In *Intermolecular Forces*; Hirschfelder, J. O., Ed.; John Wiley & Sons: New York, 1967.
(42) Boys, S. F.; Bernardi, F. *Mol. Phys.* **1970**, *19*, 553.
(43) Lide, D.T., Ed. *CRC Handbook of Chemistry and Physics*; CRC Press: Boca, Raton, 1998.
(44) Dickson, R. M.; Becke, A. D. *J. Phys. Chem.* **1996**, *100*, 16104.
(45) Hase, W. L.; Modro, S. L.; Duchovic, R. J.; Hirst, D. M. *J. Am. Chem. Soc.* **1987**, *109*, 2916.
(46) Flores, J. R.; Redondo, P. *Mol. Phys.* **1997**, *92*, 743.
(47) Kanamori, H.; Hirota, E. *J. Chem. Phys.* **1988**, *89*, 3962.
(48) Pack, R. T. *J. Chem. Phys.* **1974**, *60*, 633.
(49) Choi, S. E.; Bernstein, R. B. *J. Chem. Phys.* **1986**, *85*, 150.
(50) Nakamura, H. *Dynamics of Molecules and Chemical Reactions*; Wyatt, R. E., Zhang, J. Z. H., Eds.; Marcell Dekker: NY, 1996; Chapter 12.
(51) Gilbert, R. G.; Smith, S. C. *The Theory of Unimolecular and Recombination Reactions*; Blackwell Scientific Publications: Oxford, 1990.